AIP Conference Proceedings

Recent applications of four-body Continuum-Discretized Coupled-Channels calculations to ^{6}He reactions

Cite as: AIP Conference Proceedings **1351**, 29 (2011); https://doi.org/10.1063/1.3608932
Published Online: 10 August 2011

Manuela Rodríguez-Gallardo, and Antonio M. Moro

Recent applications of four-body Continuum-Discretized Coupled-Channels calculations to ^{6}He reactions

Manuela Rodríguez-Gallardo[*,†] and Antonio M. Moro[†]

[*]*IEM, CSIC, Serrano 123, 28006 Madrid, Spain*
[†]*Depto. FAMN, Universidad de Sevilla, Apto. 1065, 41080 Sevilla, Spain*

Abstract.
The four-body continuum-discretized coupled-channels approach using a continuum-bins scheme of discretization for three-body projectiles, that has been recently developed, is presented. The formalism is discussed and applied to reactions induced by the Borromean nucleus ^{6}He on different targets (^{27}Al, ^{64}Zn, ^{120}Sn, and ^{208}Pb), with special emphasis on the role of the Coulomb couplings.

Keywords: Few-body systems. Direct reactions. Reactions induced by unstable nuclei. Coupled-channel and distorted-wave models. Halo nuclei.
PACS: 21.45.-v,24.50.+g,25.60.-t,24.10.Eq,27.20.+n

INTRODUCTION

Exotic nuclei have been object of study in recent years due to their special properties, very different from the nuclei of the stability valley. Among the exotic nuclei, an interesting case are the so-called halo nuclei. These are weakly-bound nuclei comprising a core and one or two valence neutrons orbiting at distances larger than the typical nuclear radii. In recent years, large accelerators have been built around the world to study this kind of exotic nuclei. Simultaneously, appropriate reaction theories have been also developed to extract reliable information from the experimental data on exotic nuclei.

The continuum-discretized coupled-channels (CDCC) framework has been wide and successfully used for years to analyze experimental data on two-body weakly-bound nuclei using a three-body formalism (that is, two-body projectile plus target). Recently, the method has been extended to four-body problems (three-body projectile plus target), what allows to study reactions with three-body weakly-bound nuclei, in particular, Borromean nuclei. These nuclei has the special characteristic that none of the three binary subsystems is bound. This is the case of ^{6}He(^{4}He+n+n) or ^{11}Li(^{9}Li+n+n).

The CDCC method, for a three-body scattering problem, was developed in the 80s. The basic idea of the method, explained in detail in Refs. [1, 2], consists in expanding the states of the whole system (projectile+target) into the states of the projectile. For weakly-bound projectiles, the coupling to unbound states (that form a continuum) is relevant within the reaction dynamics. Then, we need to treat properly the continuum of the projectile. For this purpose, in the standard three-body CDCC formulation, the continuum spectrum of the projectile is truncated at a maximum excitation energy $\varepsilon_{\max}$ and the

XXXIII Brazilian Workshop on Nuclear Physics
AIP Conf. Proc. 1351, 29-38 (2011); doi: 10.1063/1.3608932

model space, from the breakup threshold to $\varepsilon_{\max}$, is then divided into intervals, where the number and positions of the intervals can depend on the properties (e.g. resonant or non-resonant) of the continuum of the system. For each such interval, or energy bin, a representative square-integrable state is constructed as a linear superposition of the two-body scattering states in the interval. The method has been enormously successful in the description of elastic and breakup observables in reactions involving weakly-bound two-body projectiles [3, 4, 5] and has been recently extended to include core excitation [6].

An alternative to treat the continuum of the projectile is to use a Pseudo-State (PS) basis. This procedure consists in diagonalizing the Hamiltonian of the system in a truncated discrete basis and taking the positive energy eigenstates as representative of the continuum. There are many PS methods in the literature. Within the CDCC framework, different bases have been used like complex-range Gaussian [7], Transformed Harmonic Oscillator (THO) [8], and Lagrange [9].

In the past decade the CDCC framework has been extended to four-body problems. Due to the difficulties in calculating the true continuum of a three-body projectile and making bins, the CDCC was first extended using PS bases like complex-range Gaussian [10, 11] and THO [12, 13]. Most recently, the binning procedure has been developed [14], providing more stable results for heavy targets.

In this work we present some recent calculations for elastic and breakup observables, for different reactions induced by the Borromean nucleus ^{6}He, obtained using the four-body CDCC formalism with the binning procedure. In Section II we explain the formal aspects of the method. In Section III we show the observables obtained for the different reactions considered. Section IV is the summary and conclusions.

FOUR-BODY CDCC FORMALISM

To describe the three-body ground and excited continuum states of the projectile we make use of a hyperspherical harmonics (HH) expansion basis [15]. This involves use of the one radial and five angular hyperspherical coordinates, $\rho, \alpha, \widehat{x}, \widehat{y}$, obtained from the normalized Jacobi coordinates $\vec{x}, \vec{y}$ (see Fig. 1) of the three bodies [15, 13]. Note that there are three different Jacobi sets. The quantum number set, β, that defines each three-body channel [13] are the hypermomentum K, the orbital angular momenta l_x and l_y in coordinates $\vec{x}$ and $\vec{y}$, their total $\vec{l} = \vec{l}_x + \vec{l}_y$, the total spin S_x of the particles associated with coordinate $\vec{x}$, and the intermediate summed angular momentum $\vec{j}_{ab} = \vec{l} + \vec{S}_x$. If the spin of the third particle, I, is assumed fixed then the total angular momentum is $\vec{j} = \vec{j}_{ab} + \vec{I}$ with projections μ. Note that, for each continuum energy ε and total angular momentum j, there will be as many independent solutions of the three-body scattering problem, as the number of outgoing channels β considered. These solutions can be chosen as the incoming channels β', but any orthogonal combination of these could be equally valid.

Based on these total angular momentum eigenstates, $\mathscr{Y}_{\beta j\mu}(\Omega)$ [13], where $\Omega \equiv (\alpha, \widehat{x}, \widehat{y})$, the bin wave functions are defined as

$$\phi^{\text{bin}}_{nj\mu}(\vec{x}, \vec{y}) = \sum_{\beta} R^{\text{bin}}_{n\beta j}(\rho) \mathscr{Y}_{\beta j\mu}(\Omega), \tag{1}$$

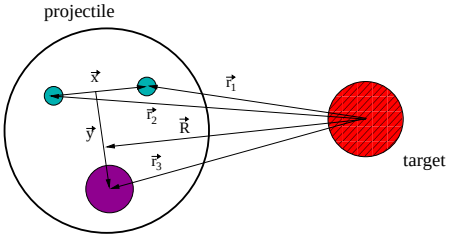

FIGURE 1. (Color online) Relevant coordinates for the scattering of a three-body projectile by a structureless target.

where the label n includes reference to the energy interval of the bin $[\kappa_1,\kappa_2]$, as well as to the set of quantum numbers β'. The functions $R^{\rm bin}_{n\beta j}(\rho)$ in Eq. (1) are the associated hyperradial wave functions,

$$R^{\rm bin}_{n\beta j}(\rho) \equiv R^{\rm bin}_{[\kappa_1,\kappa_2]\beta'\beta j}(\rho) = \frac{2}{\sqrt{\pi N_{\beta' j}}} \int_{\kappa_1}^{\kappa_2} d\kappa\, e^{-i\delta_{\beta' j}(\kappa)} f_{\beta' j}(\kappa) R_{\beta\beta' j}(\kappa,\rho), \qquad (2)$$

where $\kappa = \sqrt{2m|\varepsilon|}/\hbar$ is the momentum associated to the continuum energy ε, $R_{\beta\beta' j}(\kappa\rho)$ are the continuum hyperradial wave functions with $\delta_{\beta' j}(\kappa)$ their scattering phase shift, and $f_{\beta' j}(\kappa)$ is a weight function with $N_{\beta' j}$ its normalization constant. Note that for each j and three-body energy bin we must construct wave functions for all allowed incoming channels β'. Further, as is explicit in Eq. (1), for each n we must also construct $R^{\rm bin}_{n\beta j}(\rho)$ for all allowed outgoing channels β.

It follows that to include a large number of β' channels is a severe computational challenge, and that it is desirable to establish a hierarchy of the continuum states according to their importance to the reaction dynamics. In so doing, we may be able to describe scattering observables using only a selected set of states, the number of them depending on the reaction under study. To this end, we make use of the eigenstates of the multi-channel three-body S-matrix [16], or eigenchannels (EC), as follows. (i) For each j and continuum energy ε, the S-matrix in the β basis is diagonalized to obtain its EC, enumerated by γ, their corresponding eigenvalues $\exp[2i\delta_{\gamma j}(\kappa)]$ and eigenphases $\delta_{\gamma j}(\kappa)$. (ii) The magnitudes of these eigenphases are used to order the EC. It has been shown [14] that those EC with largest phase shifts are the most strongly coupled in the reaction dynamics, and thus a hierarchy of states can be established by such an ordering. This leads to the possibility of a truncation in the number n_{ec} of EC included and testing of the convergence with respect to this number.

The bin states given in Eq. (1) are a discrete representation of the states of the three-body projectile. From them, the four-body wavefunction of the projectile-target system, schematically depicted in Fig. 1, is formed as

$$\Psi_{JM}(\vec{R},\vec{x},\vec{y}) = \sum_{nj\mu LM_L} \phi^{bin}_{nj\mu}(\vec{x},\vec{y}) \langle LM_L j\mu | JM\rangle i^L Y_{LM_L}(\widehat{R}) \frac{1}{R} f^J_{Lnj}(R), \qquad (3)$$

where $\vec{R}$ is the coordinate from the target to the center of mass of the projectile, L is the orbital angular momentum of the projectile-target relative motion and J is the total

angular momentum, $\vec{J}=\vec{L}+\vec{j}$. The radial functions $f^J_{Lnj}(R)$ satisfy the system of coupled equations

$$\left[-\frac{\hbar^2}{2m_r}\left(\frac{d^2}{dR^2}-\frac{L(L+1)}{R^2}\right)+\varepsilon_{nj}-E\right]f^J_{Lnj}(R)+\sum_{L'n'j'} i^{L'-L}V^J_{Lnj,L'n'j'}(R)\,f^J_{L'n'j'}(R)=0, \tag{4}$$

where m_r is the reduced mass of the projectile-target system. The coupling potentials $V^J_{Lnj,L'n'j'}(R)$ are then

$$V^J_{Lnj,L'n'j'}(R)=\langle LnjJM|\widehat{V}_{pt}(\vec{r}_1,\vec{r}_2,\vec{r}_3)|L'n'j'JM\rangle, \tag{5}$$

where the ket $|LnjJM\rangle$ denotes the function $\Phi^{JM}_{Lnj}(\widehat{R},\vec{x},\vec{y})$ given by

$$\Phi^{JM}_{Lnj}(\widehat{R},\vec{x},\vec{y})=\sum_{\mu M_L}\phi^{bin}_{nj\mu}(\vec{x},\vec{y})\langle LM_L j\mu|JM\rangle Y_{LM_L}(\widehat{R}). \tag{6}$$

To calculate these coupling potentials, a multipole expansion of the projectile-target interaction is developed. The procedure is analogous to that for a three-body problem reported in Ref. [4]. We assume that the projectile-target interaction is the sum of the interactions of each particle of the projectile with the target, $V_{kt}(\vec{r}_k)$ with $k=1,2,3$. For each pair potential, an appropriate Jacobi set is chosen so that the corresponding coordinate $\vec{r}_k$ depends only on the vectors $\vec{R}$ and $\vec{y}_k$. Assuming that the potentials are central, the coefficients of the multipole expansion are generated as

$$\mathscr{V}^k_Q(R,y_k)=\frac{1}{2}\int_{-1}^{+1}V^k(r_k)P_Q(z_k)dz_k, \tag{7}$$

where $P_Q(z_k)$ is a Legendre polynomial, Q is the multipole order and $z_k=\widehat{\vec{y}}_k\cdot\widehat{\vec{R}}$ is the cosine of the angle between $\vec{y}_k$ and $\vec{R}$. So, the coupling potential can be expressed as

$$V^J_{Lnj,L'n'j'}(R)=\sum_Q(-1)^{J-j}\hat{L}\hat{L}'\begin{pmatrix}L & Q & L'\\ 0 & 0 & 0\end{pmatrix}W(LL'jj',QJ)F^Q_{nj,n'j'}(R), \tag{8}$$

where the radial form factor $F^Q_{nj,n'j'}(R)$ is

$$\begin{aligned}F^Q_{nj,n'j'}(R)&=(-1)^{Q+2j-j'}\hat{j}\hat{j}'(2Q+1)\sum_{\beta\beta'}\sum_{k=1}^{3}\sum_{\beta_k\beta'_k}N_{\beta\beta_k}N_{\beta'\beta'_k} \qquad (9)\\
&\times\ (-1)^{l_{xk}+S_{xk}+j'_{abk}-j_{abk}-I_k}\delta_{l_{xk}l'_{xk}}\delta_{S_{xk}S'_{xk}}\hat{l}_{yk}\hat{l}'_{yk}\hat{l}_k\hat{l}'_k\hat{j}_{abk}\hat{j}'_{abk}\begin{pmatrix}l_{yk} & Q & l'_{yk}\\ 0 & 0 & 0\end{pmatrix}\\
&\times\ W(l_kl'_kl_{yk}l'_{yk};Ql_{xk})W(j_{abk}j'_{abk}l_kl'_k;QS_{xk})W(jj'j_{abk}j'_{abk};QI_k)\\
&\times\ \int\!\!\int(\sin\alpha_k)^2(\cos\alpha_k)^2d\alpha_k\,\rho^5d\rho\;R^{bin}_{n\beta j}(\rho)\varphi^{l_{xk}l_{yk}}_{K_k}(\alpha_k)\mathscr{V}^k_Q(R,y_k)\varphi^{l_{xk}l'_{yk}}_{K'_k}(\alpha_k)R^{bin}_{n'\beta'j'}(\rho),\end{aligned}$$

with β_k being the set of quantum numbers in the k'th Jacobi system where the potential does not depend on x_k, and β being the set in the Jacobi system in which the states of the projectile are calculated. The matrix elements $N_{\beta\beta_k}$ transform the hyperangular, angular and spin parts of the wave functions from one Jacobi set to another. Their explicit expression as a function of the Raynal-Revai coefficients is developed in Ref. [17]. Note that Eqs. (8) and (9) are completely general, and do not depend on the nature of the basis.

APPLICATION TO ^{6}HE+TARGET REACTIONS

We apply the formalism of the preceding section to several reactions induced by the Borromean halo nucleus ^{6}He. The reactions considered, for which elastic experimental data exist, are ^{6}He+^{27}Al at 11 MeV, ^{6}He+^{64}Zn at 13.6 MeV, ^{6}He+^{120}Sn at 17.4 MeV, and ^{6}He+^{208}Pb at 22 MeV. Note that each target has a mass approximately twice that of previous target and the energies in the laboratory frame are near the Coulomb barrier. So, a study of this set of reactions can give us a insight on the role of the Coulomb interaction as the mass of the target increases.

Here we use the same structure model for the three-body system ^{6}He, as in Refs. [12, 13, 14]. The nucleus is treated as a three-body system of an inert α particle core and two valence neutrons. A notable property of ^{6}He is that none of its binary sub-systems bind, while the three-body system has a single bound state with binding energy of 0.973 MeV and total angular momentum $j^\pi = 0^+$. Its low-lying continuum spectrum is dominated by a narrow $j^\pi = 2^+$ resonance, 0.825 MeV above threshold. The Hamiltonian includes two-body potentials plus an effective three-body potential. The ^{6}He ground-state and continuum wavefunctions are generated using the codes FACE [17] and STURMXX [18]. The maximum hypermomentum used was $K_{\max} = 8$. The parameters of the three-body interaction are adjusted to reproduce the ground-state separation energy and matter radius and the resonance energy (for $j = 1^-$ and 2^+ states). The calculated ground state energy was 0.953 MeV and the root mean squared (rms) radius was 2.46 fm (assuming a rms radius of 1.47 fm for the α particle).

The coupled-channels equations were solved using the code FRESCO [19], that reads the coupling potentials externally. We included in the calculation the states with angular momentum $j = 0^+, 1^-, 2^+$ and the projectile-target interaction multipole couplings with order $Q = 0, 1, 2$. The fragment-target interactions were represented by optical potentials which reproduce the elastic scattering at the appropriate energy. The potentials used are from the global parametrization of Koning and Delaroche [20] for the n+target subsystems. For the ^{4}He+target subsystems the choice depends on the target, being from [21] for ^{27}Al, [22] for ^{64}Zn, [23] for ^{120}Sn, and [24] for ^{208}Pb. For all these reactions we have found convergence including only the first fourth EC and discretizing the continuum into 6 and 9 bins, for each EC, for j=$0^+, 2^+$ and j=1^-, respectively. The maximum energy of ^{6}He included varies from 6 MeV for ^{6}He+^{27}Al and ^{6}He+^{64}Zn to 7 MeV for ^{6}He+^{120}Sn, and 8 MeV for ^{6}He+^{208}Pb.

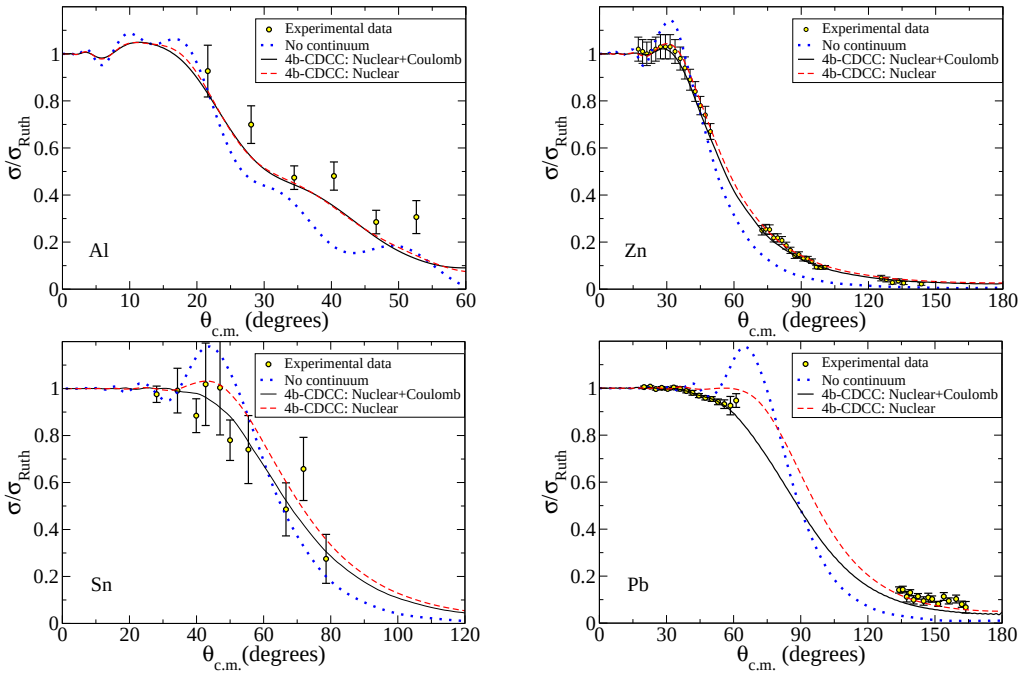

FIGURE 2. (Color online) Elastic differential cross section (ratio to Rutherford) in the center of mass frame for ^{6}He+^{27}Al at 11 MeV (top left), ^{6}He+^{64}Zn at 13.6 MeV (top right), ^{6}He+^{120}Sn at 17.4 MeV (bottom left), and ^{6}He+^{208}Pb at 22 MeV (bottom right). The experimental data are taken from Refs. [25], [22], [26], and [27] for ^{6}He+^{27}Al, ^{6}He+^{64}Zn, ^{6}He+^{120}Sn, and ^{6}He+^{208}Pb, respectively.

Elastic scattering

In Fig. 2 we show the elastic differential cross section distributions for the reactions considered. The yellow circles are the existing experimental data from Refs. [25, 22, 26, 27]. The dotted blue lines are the calculations without including the continuum. The black solid lines are the full four-body CDCC calculations including both nuclear and Coulomb interactions. Finally the dashed red lines are the full four-body CDCC calculations including only nuclear couplings (keeping the central Coulomb interaction between the colliding nuclei). We can see that in all the reactions the four-body CDCC calculations, with Coulomb and nuclear interactions, reproduces fairly well the experimental data. Only for the ^{6}He+^{208}Pb system, the experimental data at backward angles is somewhat underestimated by the calculation. We can also see the relevance of including the continuum to reproduce the experimental data. Comparing with the nuclear calculation we see that the role of the Coulomb interaction is practically negligible for the lightest target ^{27}Al whereas is crucial for the heaviest target ^{208}Pb.

Breakup

In Fig. 3 we present the breakup differential distributions as a function of the center-of-mass scattering angle. The black solid lines are the full four-body CDCC calculations

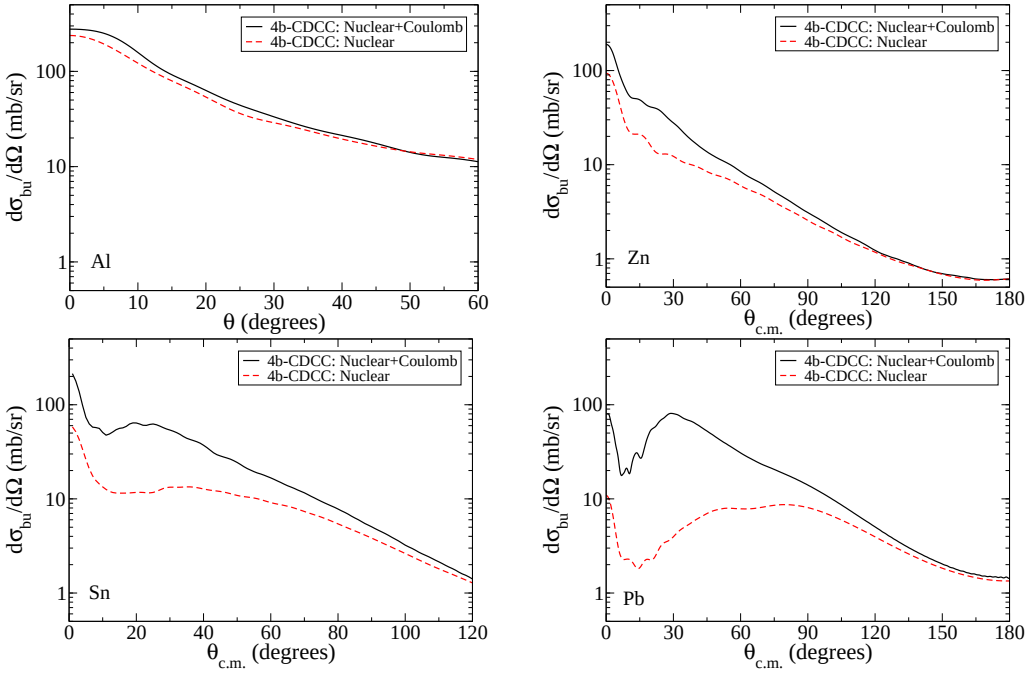

FIGURE 3. (Color online) Breakup differential cross section distribution in the center of mass frame for ^{6}He+^{27}Al at 11 MeV (top left), ^{6}He+^{64}Zn at 13.6 MeV (top right), ^{6}He+^{120}Sn at 17.4 MeV (bottom left), and ^{6}He+^{208}Pb at 22 MeV (bottom right).

TABLE 1. Total breakup and reaction cross sections.

	^{6}**He+**^{27}**Al**	^{6}**He**+^{64}**Zn**	^{6}**He**+^{120}**Sn**	^{6}**He**+^{208}**Pb**
$\sigma_{reac}^{nuc+coul}$ (mb)	1661.7	1442.9	1495.9	1389.8
$\sigma_{bu}^{nuc+coul}$ (mb)	187.09	97.06	161.85	266.28
σ_{bu}^{nuc} (mb)	166.71	56.15	67.44	70.84

including both nuclear and Coulomb interactions and the dashed red lines are the full four-body CDCC calculations including only nuclear couplings. Here we see that the Coulomb breakup is not relevant for the lightest target, whereas gets dramatically important as the mass of the target increases.

We can see this fact more clearly in Table 1 where the total reaction and breakup cross sections together with the total nuclear breakup cross section are shown. It is noticeable the large decrease of the nuclear breakup cross section with respect to the nuclear plus Coulomb breakup cross section in the case of the heaviest target, whereas both breakup cross sections are very close for the lightest target.[1]

[1] Note that the total reaction and breakup is larger for the lightest target since the energy of the reaction is well above the Coulomb barrier with respect the other three reactions.

Trivial local polarization potential

We have also extracted from the four-body CDCC calculations the so-called trivial local polarization (TLP) potential [28]. This is a local and L-independent potential which represents the overall effect of the breakup channels on the elastic scattering. This potential is constructed in such a way that the one-channel calculation performed with the potential $U_{\rm bare}(r)+U_{\rm TLP}(r)$ gives approximately the same elastic scattering as the full CDCC calculation. The bare potential, $U_{\rm bare}(r)$ is just the sum of the fragment-target interactions convoluted with the ground state density of the ^{6}He nucleus. Figure 4 shows these polarization potentials, due to Coulomb and nuclear interaction with solid black lines and nuclear with dashed lines, calculated for the different systems at different energies.

The real part of the TLP potentials is repulsive (except at very short distances where the details of this potential are probably not meaningful). This repulsive component is mainly due to nuclear couplings [29, 30, 31]. However, as the target mass increases the real part starts to exhibit a long-range negative tail at distances larger than the strong absorption radius. The effect of this long-range attractive tail is to reduce the the height of the barrier of the bare potential leading to an enhancement of the absorption [32]. This tail is known to arise from dipole Coulomb couplings and is consistent with qualitative features found in recent optical model fits of the ^{6}He+^{208}Pb data [29]. The imaginary parts of the TLP potentials are mostly absorptive. Both the real and imaginary parts extend to large distances, well beyond the strong absorption radius. These features are consistent with the findings of Mackintosh and Keeley [33] and Rusek [34].

The TLP extracted from the calculation with only nuclear couplings does not show the attractive tail for the real part, evidencing the Coulomb origin of this tail. Besides, the imaginary parts for all the targets have a longer range than in the calculation including the Coulomb couplings. This effect is larger for the heaviest target and very small for the lightest target.

SUMMARY AND CONCLUSIONS

We have presented the four-body CDCC formalism to study the reactions induced by three-body projectiles like the Borromean nucleus ^{6}He. To treat the three-body continuum of the projectile we use a continuum-bins scheme that has been recently developed. The formalism has been applied to several reactions of ^{6}He with increasing mass targets: ^{6}He+^{27}Al at 11 MeV, ^{6}He+^{64}Zn at 13.6 MeV, ^{6}He+^{120}Sn at 17.4 MeV, and ^{6}He+^{208}Pb at 22 MeV.

We have compared the elastic cross section distributions calculated with the four-body CDCC with the existing experimental data. In general, we have found a good agreement. We have compared the calculated distributions including Coulomb plus nuclear couplings with those performed including only nuclear couplings and we have found that the role of the Coulomb breakup grows drastically from the lightest to the heaviest target. The same effect is present in the breakup angular distributions.

We have also presented the TLP potentials extracted from the four-body CDCC calculations, with and without Coulomb breakup. Inclusion of Coulomb couplings has

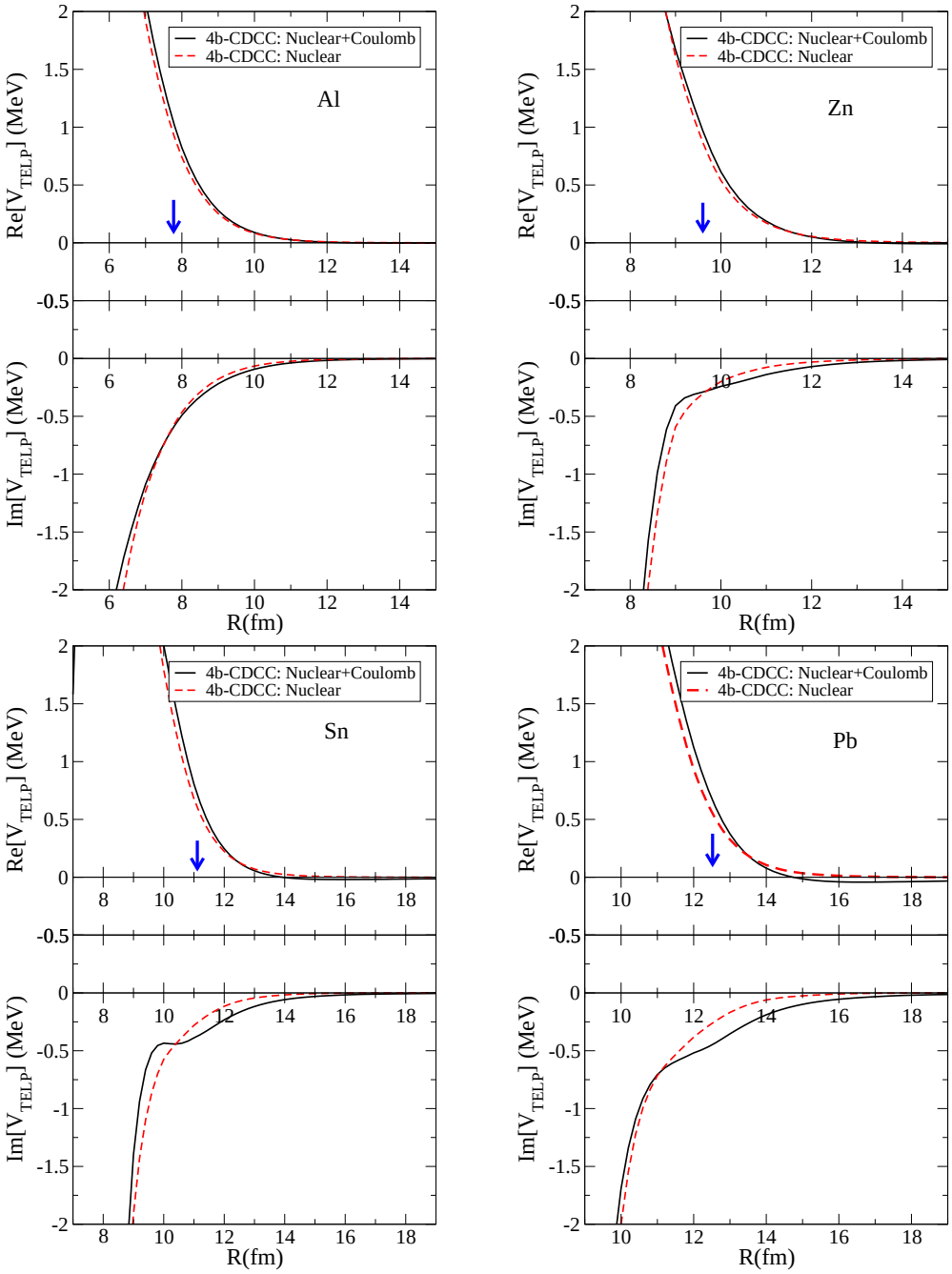

FIGURE 4. (Color online) TLP potentials extracted from the four-body CDCC calculations for ^{6}He+^{27}Al at 11 MeV (top left), ^{6}He+^{64}Zn at 13.6 MeV (top right), ^{6}He+^{120}Sn at 17.4 MeV (bottom left), and ^{6}He+^{208}Pb at 22 MeV (bottom right). The strong absorption radii are shown by arrows.

a negligible effect on the lightest target. For the heavier targets it produces a long-range attractive component in the real part of TLP and a long-range absorptive tail in the imaginary part.

ACKNOWLEDGMENTS

This work was supported by the DGICYT under Projects FPA2009-07653 and consolider CPAN.

REFERENCES

1. M. Yahiro, Y. Iseri, H. Kameyama, M. Kamimura, and M. Kawai, *Prog. Theor. Phys.* **89**, 32 (1986).
2. N. Austern, Y. Iseri, M. Kamimura, M. Kawai, G. Rawitscher, and M. Yahiro, *Phys. Rep.* **154**, 125 (1987).
3. Y. Sakuragi, M. Yahiro, and M. Kamimura, *Prog. Theor. Phys.* **89**, 136 (1986).
4. F. M. Nunes, and I. J. Thompson, *Phys. Rev. C* **59**, 2652 (1999).
5. J. A. Tostevin, F. M. Nunes, and I. J. Thompson, *Phys. Rev. C* **63**, 024617 (2001).
6. N. C. Summers, F. M. Nunes, and I. J. Thompson, *Phys. Rev. C* **74**, 014606 (2006).
7. T. Matsumoto, et al., *Phys. Rev. C* **68**, 064607 (2003).
8. A. M. Moro, F. Pérez-Bernal, J. M. Arias, and J. Gómez-Camacho, *Phys. Rev. C* **73**, 044612 (2006).
9. T. Druet, D. Baye, P. Descouvemont, and J.-M. Sparenberg, *Nucl. Phys. A* **845**, 88 (2010).
10. T. Matsumoto, E. Hiyama, K. Ogata, Y. Iseri, M. Kamimura, S. Chiba, and M. Yahiro, *Phys. Rev. C* **70**, 061601 (2004).
11. T. Matsumoto, T. Egami, K. Ogata, Y. Iseri, M. Kamimura, and M. Yahiro, *Phys. Rev. C* **73**, 051602 (2006).
12. M. Rodríguez-Gallardo, J. M. Arias, J. Gómez-Camacho, R. C. Johnson, A. M. Moro, I. J. Thompson, and J. A. Tostevin, *Eur. Phys. J. S.T.* **150**, 51 (2007).
13. M. Rodríguez-Gallardo, J. M. Arias, J. Gómez-Camacho, R. C. Johnson, A. M. Moro, I. J. Thompson, and J. A. Tostevin, *Phys. Rev. C* **77**, 064609 (2008).
14. M. Rodríguez-Gallardo, J. M. Arias, J. Gómez-Camacho, A. M. Moro, I. J. Thompson, and J. A. Tostevin, *Phys. Rev. C* **80**, 051601(R) (2009).
15. B. V. Danilin, et al., *Phys. Rev. C* **69**, 024609 (2004).
16. P. Descouvemont, E. Tursunov, and D. Baye, *Nucl. Phys. A* **765**, 370 (2006).
17. I. J. Thompson, F. M. Nunes, and B. V. Danilin, *Comput. Phys. Commun.* **161**, 87 (2004).
18. I. J. Thompson, *Unpublished. Users manual available from the author* (2002).
19. I. J. Thompson, *Comp. Phys. Rep.* **7**, 167 (1988).
20. A. J. Koning, and J. P. Delaroche, *Nucl. Phys. A* **713**, 231 (2003).
21. S. Kailas, *Reference Input Parameter Library (RIPL-2), available online at http://www-nds.iaea.org/RIPL-2/* (2003).
22. A. D. Pietro, et al., *Phys. Rev. C* **69**, 044613 (2004).
23. V. Avrigeanu, P. E. Hodgson, and M. Avrigeanu, *Phys. Rev. C* **49**, 2136 (1994).
24. A. R. Barnett, and J. S. Lilley, *Phys. Rev. C* **9**, 2010 (1974).
25. E. A. Benjamim, et al., *Phys. Lett. B* **647**, 30 (2007).
26. P. N. de Faria, et al., *Phys. Rev. C* **81**, 044605 (2010).
27. A. M. Sánchez-Benítez, et al., *Nucl. Phys. A* **803**, 30 (2008).
28. I. J. Thompson, M. A. Nagarajan, J. S. Lilley, and M. J. Smithson, *Nucl. Phys. A* **505**, 84 (1989).
29. J. P. Fernández-García, M. Rodríguez-Gallardo, M. A. G. Alvarez, and A. M. Moro, *Nucl. Phys. A* **840**, 19 (2010).
30. Y. Sakuragi, *Phys. Rev C* **35**, 2161 (1987).
31. M. Yahiro, M. Nakano, Y. Iseri, and M. Kamimura, *Prog. Theor. Phys.* **67**, 1467 (1982).
32. O. Kakuee, et al., *Nucl. Phys. A* **765**, 294 (2006).
33. R. S. Mackintosh, and N. Keeley, *Phys. Rev. C* **79**, 014611 (2009).
34. K. Rusek, *Eur. Phys. J. A* **41**, 399 (2009).